Biophysical Journal Volume 104 June 2013 2410–2418

Small-Molecule Photostabilizing Agents are Modifiers of Lipid Bilayer Properties

Jose L. Alejo, Scott C. Blanchard, and Olaf S. Andersen*
Department of Physiology and Biophysics, Weill Cornell Medical College, New York, New York

ABSTRACT Small-molecule photostabilizing or protective agents (PAs) provide essential support for the stability demands on fluorescent dyes in single-molecule spectroscopy and fluorescence microscopy. These agents are employed also in studies of cell membranes and model systems mimicking lipid bilayer environments, but there is little information about their possible effects on membrane structure and physical properties. Given the impact of amphipathic small molecules on bilayer properties such as elasticity and intrinsic curvature, we investigated the effects of six commonly used PAs—cyclooctatetraene (COT), *para*-nitrobenzyl alcohol (NBA), Trolox (TX), 1,4-diazabicyclo[2.2.2]octane (DABCO), *para*-nitrobenzoic acid (pNBA), and n-propyl gallate (nPG)—on bilayer properties using a gramicidin A (gA)-based fluorescence quench assay to probe for PA-induced changes in the gramicidin monomer↔dimer equilibrium. The experiments were done using fluorophore-loaded large unilamellar vesicles that had been doped with gA, and changes in the gA monomer↔dimer equilibrium were assayed using a gA channel-permeable fluorescence quencher (Tl^+). Changes in bilayer properties caused by, e.g., PA adsorption at the bilayer/solution interface that alter the equilibrium constant for gA channel formation, and thus the number of conducting gA channels in the large unilamellar vesicle membrane, will be detectable as changes in the rate of Tl^+ influx—the fluorescence quench rate. Over the experimentally relevant millimolar concentration range, TX, NBA, and pNBA, caused comparable increases in gA channel activity. COT, also in the millimolar range, caused a slight decrease in gA channel activity. nPG increased channel activity at submillimolar concentrations. DABCO did not alter gA activity. Five of the six tested PAs thus alter lipid bilayer properties at experimentally relevant concentrations, which becomes important for the design and analysis of fluorescence studies in cells and model membrane systems. We therefore tested combinations of COT, NBA, and TX; the combinations altered the fluorescence quench rate less than would be predicted assuming their effects on bilayer properties were additive. The combination of equimolar concentrations of COT and NBA caused minimal changes in the fluorescence quench rate.

INTRODUCTION

Fluorescence techniques such as bulk fluorometry, fluorescence correlation spectroscopy, wide-field, scanning confocal, total internal reflection fluorescence, and super-resolution microscopy rely on stable fluorescent species (1–4). The use of such fluorophores, which include organic dyes, fluorescent proteins, inorganic quantum dots, and nanocrystals, is limited by stochastic blinking and irreversible photobleaching. Blinking is an illumination intensity-dependent, reversible loss of fluorescence that leads to dark states. Photobleaching is an irreversible loss of fluorescence arising from chemical damage of the fluorogenic center. As oxygen and oxygen-generated molecular species contribute directly to photobleaching (5–7), oxygen-scavenging systems are typically employed to extend fluorophore lifetimes (4). However, such efforts tend to increase the prevalence of long-lived dark states because oxygen is also an effective triplet state quencher (TSQ) (5,8). It thus becomes important to control these photophysical processes, in order to enhance dye brightness, stability, and lifetime. To this end, small-molecule photostabilizing, or protective agents (PAs), such as the antioxidant Trolox, the TSQ cyclooctatetraene, and the oxidant *para*-nitrobenzoic acid, are typically employed to suppress the prevalence and duration of triplet dark states (1–4,8–12).

Many of these compounds are rather hydrophobic—the calculated logarithm of the octanol/water distribution coefficient at pH 7.4 ($c\mathrm{Log}D$) ranges from ~–1.3 for *para*-nitrobenzoic acid to ~2.5 for cyclooctatetraene (see Table S1 in the Supporting Material)—and they are employed at millimolar concentrations. These compounds thus may have undesired effects because they partition into the bilayer, thereby altering bilayer properties (13–15). This is important because membrane proteins occur in different conformations, with different organization of the bilayer-spanning domains (16), and hydrophobic interactions between bilayer proteins and their host bilayers couple conformational changes of bilayer-spanning proteins to local deformations of the bilayer adjacent to the proteins (16–19). This bilayer deformation has an associated energetic cost, the bilayer deformation energy (ΔG_{def})—and the difference in bilayer deformation energy between two protein conformations (I and II) becomes the bilayer contribution ($\Delta G^{\mathrm{I}\rightarrow\mathrm{II}}_{\mathrm{bilayer}} = \Delta G^{\mathrm{II}}_{\mathrm{def}} - \Delta G^{\mathrm{I}}_{\mathrm{def}}$) to the overall free energy cost of the protein conformational change (16). Adsorption of amphiphiles at the bilayer interface (or partitioning into the bilayer core) with the associated changes in

Submitted August 7, 2012, and accepted for publication April 11, 2013.
*Correspondence: sparre@med.cornell.edu
Editor: Huey Huang.

0006-3495/13/06/2410/9 $2.00
http://dx.doi.org/10.1016/j.bpj.2013.04.039

bilayer physical properties (such as changes in thickness, intrinsic curvature, and the associated elastic moduli), together with this energetic coupling, provides a general mechanism for nonspecific alterations in membrane protein function (20–24). Because the PAs listed above have been employed in fluorescence-based studies on live cells (25–32) and biomembrane model systems (33–38), we explored whether commonly used PAs such as TX (Trolox), nPG (n-propyl gallate), DABCO (1,4-Diazabicyclo[2.2.2]octane), COT (cyclooctatetraene), NBA (*para*-nitrobenzyl alcohol), pNBA (*para*-nitrobenzoic acid), and PCA (protocatechuic acid) (their structures are shown in Fig. S1 in the Supporting Material and their physicochemical properties are summarized in Table S1) alter lipid bilayer properties, as sensed by bilayer-spanning channels, using the gramicidin A (gA) channels as probes.

gA channels have been employed extensively as probes to explore how changes in membrane composition, including the adsorption of small amphiphiles, alter bilayer properties using electrophysiological (18,20–24,39) and stopped-flow fluorescence (40,41) methods. gA channels are suitable probes for changes in bilayer properties because channel formation in a bilayer with a hydrophobic thickness (3–5 nm) that exceeds the channel's hydrophobic length (~2.2 nm (42,43)) causes a local decrease in bilayer thickness to match the channel length (44); see Fig. 1. (An alternative scheme, in which the gA current transitions were proposed to represent closed↔open transitions in stable dimers, was proposed recently in Jones et al. (45). This scheme is at odds with 40 years of studies. (Much of the early evidence is summarized in Andersen et al. (46), which show the gA channels form by the bimolecular association/dissociation of gA subunits, and the results of Jones et al. can be accounted for by exchange of gA between different bilayer leaflets, which was proposed long ago (47,48), and demonstrated experimentally (49). We therefore do not consider this model.) As is the case for membrane proteins, the bilayer deformation associated with gA channel formation has an energetic cost, and the difference in the bilayer deformation energy for the monomers (M) and the bilayer-spanning dimers (D) becomes the bilayer contribution $(\Delta G^{M\to D}_{bilayer} = \Delta G^{D}_{def} - \Delta G^{M}_{def})$ to the free energy of dimerization. Changes in lipid bilayer properties, whether it be changes in hydrophobic thickness, intrinsic monolayer curvature, or the associated elastic moduli (caused by adsorption at the bilayer/solution interface or partitioning into the bilayer core), e.g., Evans et al. (13), and Zhelev (50), will alter the $\Delta G^{M\to D}_{bilayer}$ contribution to the free energy gA formation and be observed as changes in channel activity (the time-averaged channel density in the bilayer). It is thus possible to use gA channels to probe for, e.g., PA-induced changes in bilayer properties.

In this study, the changes in gA channel activity were monitored using a scalable gramicidin-based fluorescence quench method (40) using gA-doped large-unilamellar vesicles (LUVs) loaded with the fluorophore ANTS (8-aminonaphthalene-1,3,6-trisulfonate) (Fig. 2), which allows for the determination of the PA-dependent changes in $\Delta G^{M\to D}_{bilayer}$. When the ANTS-loaded LUVs are mixed with the gA channel-permeant fluorescence quencher Tl^+ in a stopped-flow spectrofluorometer, the changes in the time course of fluorescence quenching becomes a measure of the changes of the average number of gA channels per vesicle. Using this strategy, we find that TX, NBA, and pNBA, at millimolar (1–4 mM) concentrations, caused comparable increments (up to ninefold) in the average gA activity. COT, again at millimolar (1–4 mM) concentrations, caused a slight decrease in the average gA activity (up to ~50%), whereas nPG caused large (more than 10-fold) activity increments at submillimolar (0.2–0.8 mM) concentrations. DABCO did not alter gA activity at the highest concentration tested (4 mM), suggesting it does not alter bilayer properties. Knowing the effects of these and other additives on lipid bilayer properties is anticipated to inform decisions about their use in fluorescence studies on live cells and model membrane systems.

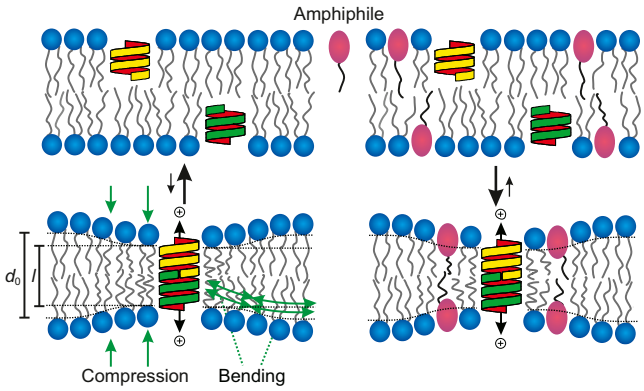

FIGURE 1 Using gA channels as probes for changes in lipid bilayer properties. Bilayer-spanning gA channels form by transmembrane dimerization of two $\beta^{6.3}$-helical subunits, with a hydrophobic length that is less than the hydrophobic length of the unperturbed bilayer. (*Left*) Because the channel length (l) is less than the unperturbed bilayer thickness (d_0), there is a hydrophobic mismatch; the bilayer will adapt to minimize the exposure of hydrophobic residues to water. This adaptation involves local compression of the bilayer hydrophobic core and bending of the bilayer/solution interface. Channel formation thus will incur an energetic cost, meaning that the energetic cost of channel formation varies with changes in lipid bilayer properties. (*Right*) In bilayers that have been modified by the adsorption of amphiphiles at the bilayer/solution interface, the bilayer has additional degrees of freedom in terms of how it adapts to a channel-bilayer hydrophobic mismatch because the amphiphiles may redistribute between the membrane and the aqueous phases, which will tend to reduce the magnitude of the energetic cost of channel formation such that the gA monomer↔dimer equilibrium will tend to be shifted toward the conducting dimers. (In some cases, e.g., our results with COT, the compound increases the energetic cost of channel formation and shifts the gA monomer↔dimer equilibrium toward the nonconducting monomers.)

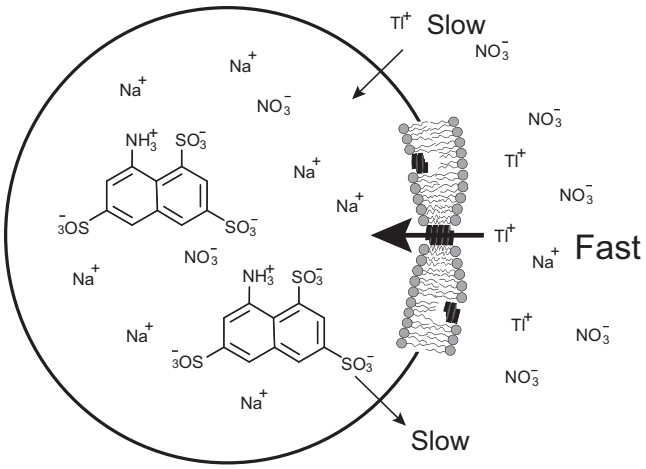

FIGURE 2 Testing for bilayer-modifying effects using stopped-flow spectrofluorometry. ANTS-loaded LUVs formed with gramicidin A (gA) are exposed to the quencher Tl^+. Over the experiment timescale of 1 s, ANTS and $TlNO_3$ are only slightly permeant through the lipid bilayer, whereas gA channels are highly Tl^+ permeable. The rate of Tl^+ influx is proportional to the number of conducting channels in the LUV membrane. (Expanded view on the *right*) Segment of the lipid bilayer with the two major gA conformers: nonconducting monomers and conducting dimers. Modified after (40).

MATERIALS AND METHODS

Materials

Unless otherwise noted, all reagents were from Sigma (St. Louis, MO), the gramicidin used was the natural mixture of gramicidins, which is predominantly gramicidin A. $DC_{22:1}PC$ (1,2-$C_{22:1}$-*sn*-glycero-3-phosphocholine) was from Avanti Polar Lipids (Birmingham, AL). ANTS (8-Aminonaphthalene-1,3,6-trisulfonate) disodium salt was from Invitrogen (Eugene, OR). NBA (para-nitrobenzyl alcohol), nPG (n-Propyl gallate), and COT (cyclooctatetraene)) were dissolved in DMSO (dimethyl sulfoxide) to a final concentration of 1 M. PCA (protocatechuic acid, 3,4-Dihydroxybenzoic acid) was dissolved in deionized water to a final concentration of 100 mM, and the pH was adjusted to 7.0 using HNO_3. DABCO (1,4-Diazabicyclo[2.2.2]octane) was dissolved in water, and the pH was adjusted to 7.0 with HNO_3; the final concentration was 1 M. A buffered TX (Trolox) solution was prepared by dissolving TX in DMSO (0.5 M) followed by addition of HEPES, $NaNO_3$, and deionized water to yield a final composition: 135 mM $NaNO_3$, 10 mM HEPES, and 10 mM TX at pH 7.0. A buffered pNBA (*para*-nitrobenzoic acid) solution was prepared by dissolving pNBA, HEPES, and $NaNO_3$ in deionized water to a final composition of 130 mM $NaNO_3$, 10 mM HEPES, and 20 mM pNBA at pH 7.0. The actual TX and pNBA concentration was adjusted by mixing the TX/pNBA-containing buffer with the TX/pNBA-free suspension of LUVs in extravesicular buffer (140 mM $NaNO_3$ and 10 mM HEPES at pH 7.0).

LUV preparations

The fluorophore ANTS was loaded into LUVs using hydration/mini-extrusion (51). For each batch of LUVs, the lipid and gA solution was dried under nitrogen and dried further in a desiccator under vacuum overnight. The lipid film was hydrated in 100 mM $NaNO_3$, 25 mM ANTS (Na^+ salt), and 10 mM HEPES, pH 7.0 at room temperature overnight, adjusting the volume to give a 10 mM lipid, 5.2 μM gA suspension. The suspension was sonicated in a Bransonic 3510 bath sonicator (Branson Ultrasonics, Danbury, CT) at 90 W power for 1 min, subjected to five freeze-thaw cycles and extruded 21 times at room temperature with an Avanti Polar Lipids mini-extruder and 0.1 μm polycarbonate membrane filter. Unencapsulated ANTS was removed using a PD-10 desalting column (GE Healthcare, Piscataway, NJ), and the vesicle stock solution (~5 mM lipid) was stored in the dark at 12.5°C for a maximum of seven days. For the fluorescence experiments, the ANTS-loaded LUV stock solution was diluted 1:20 with extravesicular solution buffer of 140 mM $NaNO_3$ and 10 mM HEPES at pH 7.0. (HEPES has some effects on lipid bilayer properties at high, 100-mM, concentrations, but is inert at 10 mM (52).) Electron microscopy imaging of such samples showed that the vesicle size is normally distributed with an average vesicle diameter of ~150 $\pm$ 50 nm (data not shown).

Fluorescence spectroscopy

The time course of ANTS fluorescence quenching was measured at 25°C using a SX.20 stopped-flow spectrofluorometer (Applied Photophysics, Leatherhead, UK) with a 150 W Xenon lamp and two-sample-rapid mixing unit with machine dead time ~1.5 ms. The excitation was at 352 nm and the fluorescence was recorded above 450 nm with ProData control software and high-pass filter from Applied Photophysics, with a sampling rate of 5000 points/s. For each sample, the additives were incubated with the LUV suspension for 10 min and several (at least five) 1-s mixing trials were recorded. In each buffer (fluorescence baseline) trial, the vesicle solution was mixed with extravesicular solution buffer (140 mM $NaNO_3$ and 10 mM HEPES at pH 7.0). In each quenching trial the vesicle solution was mixed with quenching buffer (50 mM $TlNO_3$, 94 mM $NaNO_3$, and 10 mM HEPES at pH 7.0).

Data analysis

To quantify the PA-induced changes in the time course of fluorescence quenching, the kinetics of ANTS quenching by Tl^+ must be considered. For a single vesicle with a fixed number of conducting channels, the Tl^+ influx can be approximated as a first-order process. The size distribution of the vesicles, however, leads to different-sized vesicles filling with Tl^+ at varying rates—and initially active pores may deactivate and new channels may form over the time course of the experiment. For a single vesicle, with a single conducting channel, the time course of fluorescence quenching is given by

$$E(t) = \frac{F(t)}{F_0} = \frac{1}{1 + KQ(\infty)[1 - \exp\{-kt\}]}, \qquad (1)$$

where $F(0)$ and $F(t)$ denote the fluorescence at time 0 (in the absence of quencher) and at time t; $E(t)$ is the normalized fluorescence; K is the Stern-Volmer quenching constant; $Q(\infty)$ is the intravesicular quencher concentration at time infinity (= the extravesicular quencher concentration); and k is the rate constant for quencher influx ($k = \sigma/Vol$, where Vol is the LUV volume and σ is the quencher's single-channel permeability coefficient). In this case, the initial rate of quenching (at $t = 0$) is given simply by

$$\left.\frac{dE(t)}{dt}\right|_{t=0} = -kKQ(\infty).$$

For a mixed population of vesicles, where the different populations (1, 2,...) have different influx rates (k_1, k_2,…), the time course of quencher influx becomes the weighted sum of exponential terms of the form of Eq. 1, with weights that reflect distribution of vesicle size and the number of conducting channels in the vesicle membrane (as well as the channel formation rate and lifetime),

$$E(t) = \frac{F(t)}{F_0} = \sum_i \frac{w_i}{1 + KQ(\infty)[1 - \rho_i(t)]}, \qquad (2)$$

where w_i is the volume fraction and ρ_i is the retention function (53) of the vesicles in population i (vesicles of the same size will be distributed across different populations based on the number of channel in their membrane). Equation 2 can be expressed as a sum of exponential terms (see Methods in the Supporting Material) such that

$$E(t) = 1 - B + B\sum_{i,m,n=1}\Psi(i,m,n)e^{-k_{imn}t}, \quad (3)$$

where $B = KQ(\infty)/[1 + KQ(\infty)]$ and $\Psi(i,m,n)$ denotes the frequency distribution of the exponential terms, and the indices i, m, and n denote the vesicles size distribution, the pore distribution across vesicles, and a series expansion of the $w_i/(1+KQ(\infty)[1-\rho_i(t)])$ terms in Eq. 2 (see Methods in the Supporting Material and Eq. 15). $\Psi(i,m,n)$ accounts for the distribution of vesicle sizes, as well as the distribution of conducting channels among the vesicles. Such infinite sums of exponential terms can often be represented in a mathematically efficient manner by a so-called modified stretched exponential (54,55)

$$I(t) = \exp\left[1 - \left(\frac{1+t}{t_1}\right)^{\beta}\right], \quad (4)$$

where t_1 is a parameter with units of time, and β ($0 < \beta \leq 1$) is a parameter that describes the dispersity of the distribution of vesicle sizes and number of gA channels/vesicle. The experimental time course of fluorescence quenching thus can be can be described as

$$E(t) = \frac{F(t)}{F_0} = 1 - B + B\exp\left[1 - \left(\frac{1+t}{t_1}\right)^{\beta}\right], \quad (5)$$

with the initial rate of fluorescence quenching given by $dE(t)/dt|_{t=0} = -B\beta/t_1$.

For the analysis, the fluorescence intensities $F(t)$ were normalized to the initial (first 2–10 ms) average fluorescence in the absence of quencher, F_0. For each experiment, Eq. 5 was fitted to the initial 1 s of each quenching repeat (see Fig. 3 *B*) using a nonlinear least-squares fit implemented in the software MATLAB (The MathWorks, Natick, MA) to provide estimates for β and t_1 (see Table S2). The initial quench rate ($\langle k\rangle$) then was estimated as the initial rate of decay of the modified stretched exponential (Eq. 5, and see Berberan-Santos et al. (55))

$$\langle k\rangle = \frac{\beta}{t_1}, \quad (6)$$

where the variation in $\langle k\rangle$ reports on PA-induced changes in gA activity. More specifically, approximating the theoretical average exponential decay rate (obtained from Eq. 3) to that obtained from the fits as Eq. 6, we obtain the relation (see Methods in the Supporting Material)

$$r = \frac{\langle k\rangle - \langle k\rangle_0}{\langle k\rangle_{ref} - \langle k\rangle_0} = \frac{(\beta/t_1) - (\beta/t_1)_0}{(\beta/t_1)_{ref} - (\beta/t_1)_0} \cong \frac{p}{p_{ref}}, \quad (7)$$

where $\langle k\rangle$ is the initial influx rate in the presence of the bilayer modifier; $\langle k_{ref}\rangle$ is the initial rate with no added modifier; $\langle k_0\rangle$ is the average influx rate in the absence of gA; and p and p_{ref} are the average number of gA channels/vesicle in the presence and absence of the PA. This normalized rate was used to quantify the changes in gA activity. In the limit $\langle k\rangle_0/\langle k\rangle \to 0$,

$$r \cong \frac{\langle k\rangle}{\langle k\rangle_{ref}}.$$

Assuming that the added compounds alter only the bilayer contribution to the free energy of the gA monomer↔dimer equilibrium, we estimate the modifier-induced changes in $\Delta\Delta G^{M\to D}_{bilayer}$ as in Lundbaek et al. (16):

$$\Delta\Delta G^{M\to D}_{bilayer} = \Delta G^{M\to D}_{bilayer,PA} - \Delta G^{M\to D}_{bilayer,ref} \cong -k_BT\ln\{r\}. \quad (8)$$

RESULTS

Tl^+ permeates lipid bilayers slowly but is very permeant through conducting gA channels. The rate of fluorescence quenching hence is proportional to gA channel activity (average number of conducting channels in the vesicle membrane), which varies with changes in bilayer properties. Such changes may be caused by amphiphiles that adsorb at the bilayer/solution interface and thereby alter lipid bilayer properties and thus the energetic cost of bilayer adaptation required for hydrophobic matching to the bilayer-spanning gA channel. Fig. 3 shows the time courses of fluorescence quenching for vesicles incubated with increasing amounts of TX. In the absence of the quencher, Tl^+, the ANTS-filled LUVs fluoresce stably over the 1 s record (Fig. 3 *A*, *top curve*). In gA-free LUVs, Tl^+ produces a small, immediate drop in fluorescence (Fig. 3 *A*, *second curve* from *top*) due to the quenching of unencapsulated ANTS, as well as a slow decay most likely due to $TlNO_3$ ion-pair (56,57) leakage across the bilayer. The time course of this slow fluorescence

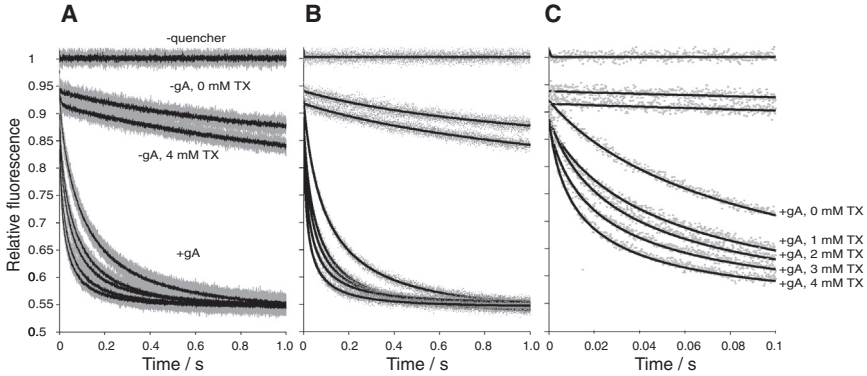

FIGURE 3 Effect of Trolox (TX) on the time course of ANTS fluorescence quenching. (*A*) (*Traces*) Normalized fluorescence time signal over 1 s; (*shaded dots*) results from all repeats ($n > 5$ per condition); (*solid lines*) average of all repeats. (*Top trace*) Results in the absence of the quencher Tl^+; (*next two traces*) results in the absence of gA with Tl^+ and without or with the highest TX concentration employed (4 mM); (*lower five fluorescence time courses*, from *top* to *bottom*) gA-containing vesicles incubated with 0, 1, 2, 3, and 4 mM TX. (*B*) (*Dots*) Results from a single repeat for each condition; (*lines*) modified stretched exponential fits to those repeats. (*C*) The first 100 ms of the fluorescence time courses and their corresponding fits.

quenching is comparable in the absence and presence of 4 mM TX, meaning that TX neither promotes Tl^+ leakage across the bilayer nor induces membrane destabilization. In the presence of gA, TX increases the fluorescence quench rate in a concentration-dependent manner (Fig. 3, *curves* 4–7 from the *top*). Fig. 3, *B* and *C*, shows the fits (to Eq. 5) of the fluorescence quench time courses for various concentrations of TX.

Similar results were obtained with most of the other PAs examined. Fig. 4 summarizes our results on the bilayer-modifying effects of the PAs over the concentration ranges that are used in single-molecule fluorescence microscopy. The β, t_1, and $\langle k \rangle$ parameters determined from the fits of Eq. 5 to the experimental results are summarized in Table S2. Changes in the time course of quenching are reflected primarily as changes in t_1, whereas β usually varies little. The PA effects on the bilayer properties were quantified by the relative change in the rate of fluorescence quenching, r (Eq. 7), which provides an estimate of the relative change in the average number of gA channels/vesicle in the presence and absence of the PA. At low millimolar concentrations (1–4 mM), TX, NBA, and pNBA alter bilayer properties, as sensed by gA channels, with up to ninefold increases in the average dimer ratio over the millimolar (1–4 mM) concentration range.

TX partly degrades in buffer to form a quinone derivative (58). TX on its own therefore functions as a reducing/oxidizing system (ROXS), where TX itself is a reductant and the TX-quinone is the oxidant (58). Prolonged (up to 36 h) room temperature aging of the dissolved TX had no effect on our observations, indicating that the bilayer alterations caused by TX are insensitive to TX-quinone formation. nPG is the most potent bilayer modifier, increasing the average channel density more than 10-fold in the submillimolar (0.2–0.8 mM) concentration range. COT, in contrast, decreased gA channel activity, reducing the average channel density by 10–50% over the millimolar (1–4 mM) concentration range. The strong base DABCO had no effect on gA activity. PCA (protocatechuic acid), part of a widely used oxygen scavenging system (5), similarly was found to have no effect on bilayer properties as sensed by gA channels (data not shown).

When comparing the structurally related NBA (*para*-nitrobenzyl alcohol) and pNBA (*para*-nitrobenzoic acid) at pH 7, where pNBA is almost completely deprotonated (pKa = 3.4 (59)), pNBA is a weaker bilayer modifier than its alcohol counterpart (Fig. 4), likely owing to its reduced partitioning into the lipid bilayer at neutral pH (the interfacial PK of weak acids tend to be 2–2.5 pH units higher than their bulk pKa (60–62)). To test this hypothesis, we also performed experiments also at pH 4, where ~20% of the pNBA is expected to be protonated. The normalized fluorescence quench rate induced by 3 mM pNBA increased from 2.4 ± 0.2 at pH 7 to 3.7 ± 0.1 at pH 4, reflecting the increased bilayer partitioning of protonated pNBA.

The PA effects on the bilayer energetics were quantified using Eq. 8. The results over the relevant concentration ranges are summarized in Fig. 5. The energy differences vary widely among the different compounds and concentrations, reaching values of 2 k_BT. $\Delta\Delta G^{M\rightarrow D}_{bilayer}$ for all the membrane-active PAs (TX, NBA, nPG, COT, and pNBA) varies linearly ($r^2 > 0.98$ for each compound) as a function of concentration across the ranges explored. The slopes of the $\Delta\Delta G^{M\rightarrow D}_{bilayer}$-[PA] relations vary in both magnitude and

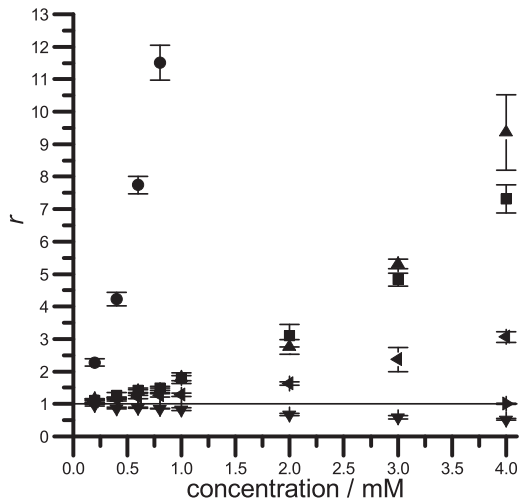

FIGURE 4 Normalized gA activation-induced fluorescence quenching rates ($r = \langle k \rangle / \langle k \rangle_{ref}$); see Eq. 7, quantifying the effect of photostabilizing agents on lipid bilayer properties. The symbols denote: ▼, COT; ▶, DABCO; ▲, NBA; ◀, pNBA; ●, nPG; and ■, TX. (*Straight line* at $r = 1$) Guide to the eye.

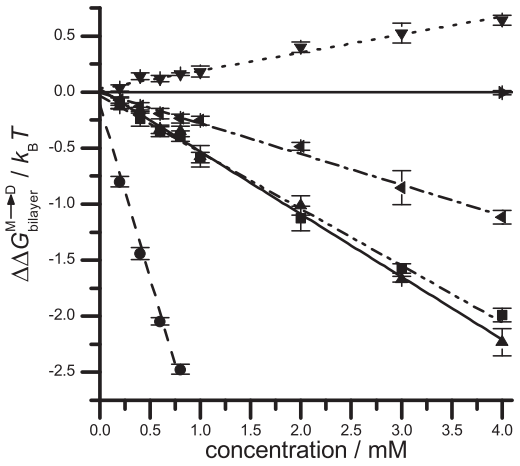

FIGURE 5 Shifts in the bilayer contribution to the energetic cost of gA dimer formation due to the influence of various PAs at the specified concentrations. The symbols denote: ▼, COT; ▶, DABCO; ▲, NBA; ◀, pNBA; ●, nPG; and ■, TX. (*Dotted line*) Linear fits to the data for COT ($y = 0.160x + 0.03$, $r^2 = 0.982$); (*dot-dashed line*) for pNBA ($y = -0.275x - 0.005$, $r^2 = 0.994$); (*dot-dot-dashed line*) for TX ($y = -0.505x - 0.033$, $r^2 = 0.995$); (*solid line*) for NBA ($y = -0.558x + 0.026$, $r^2 = 0.996$); and (*dashed line*) for nPG (slope = –3.096x – 0.1134, $r^2 = 0.988$).

sign, from large (–3.1 k_BT/mM for nPG) to moderate (0.16 k_BT/mM for COT).

Given the linear $\Delta\Delta G^{M\rightarrow D}_{bilayer}$-[PA] relations, we explored whether the bilayer effects of different PAs were additive; they are not. Fig. 6 shows results obtained with equimolar mixtures of COT+NBA+TX (4), as well as equimolar binary mixtures of COT+NBA, COT+TX, and NBA+TX. As was the case when only one PA was present, the $\Delta\Delta G^{M\rightarrow D}_{bilayer}$-[PA] relations were linear ($r^2 > 0.9$) for each combination (with the exception of the COT+NBA mix, which oscillated around zero), but the changes in $\Delta G^{M\rightarrow D}_{bilayer}$ were consistently less than would be predicted from the experiments with the individual compounds (see Fig. S7). The combination of 1 mM COT, 1 mM NBA, and 1 mM TX, for example, changed $\Delta G^{M\rightarrow D}_{bilayer}$ by –0.63 ± 0.06 k_BT, whereas the sum of the changes produced by 1 mM of COT, NBA, or TX when added individually was –0.97 ± 0.19 k_BT. This disparity increased with increasing PA concentration, suggesting that it would be advantageous to use combinations of PAs to reduce the risk of unwanted bilayer effects. We note, in particular, that the COT+NBA mixture produced no changes in the fluorescence quench rate at the highest concentrations tested (2 mM of each PA).

DISCUSSION

We show that commonly used fluorescence stabilizers alter lipid bilayer properties at the concentrations in which these reagents typically are employed in fluorescence imaging studies. The photostabilizing agents studied were chosen for their different chemical functionalities (see Fig. S1), as well as their reported capacity to improve dye stability by serving as TSQs, antioxidants, ROXS components, or singlet oxygen quenchers. For example, DABCO, used as an antifading agent in fluorescence microscopy and as a stabilizer of dye lasers, likely exerts its actions by a combination of triplet state and singlet oxygen quenching (3,63,64). The antioxidant nPG has been shown to slow photobleaching in fluorescence microscopy applications (2,65–67), including live cell studies (68–71). TX, which initially was thought to function as an antioxidant and has been widely employed as an antioxidant in different cell treatments (72–75), partly degrades to form a quinone derivative (58). However, prolonged (36 h) room temperature aging of the dissolved TX had no effect on our observations, indicating that the bilayer alterations caused by TX are insensitive to any TX-quinone formation. Both NBA and pNBA have been employed as PA, including as oxidants in ROXS systems (4,12) and COT has been used as a TSQ (2,4,31). Additionally, PCA is an additive used in conjunction with the protocatechuate-3,4-dioxygenase oxygen-scavenging system (4,5,76). These compounds usually are employed in the millimolar regime, concentrations at which they alter lipid bilayer properties, as reported by changes in gA channel activity.

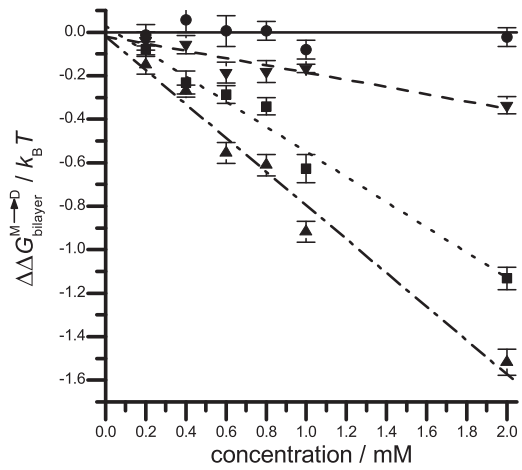

FIGURE 6 Shifts in the bilayer contribution to the energetic cost of gA dimer formation due to the influence of various PA combinations at the specified concentrations. The symbols denote: ■, COT+NBA+TX; ●, COT+NBA; ▼, COT+TX; and ▲, NBA+TX. The concentrations indicated on the abscissa denote the concentration of each of the PAs, which were added as equimolar mixtures. (*Straight line* at $\Delta\Delta G_{bilayer} = 0$) Guide to the eye. (*Dotted line*) Linear fits for COT+NBA+TX ($y = –0.578x + 0.028$, $r^2 = 0.91$); (*dot-dashed line*) NBA+TX ($y = –0.776x – 0.02$, $r^2 = 0.98$); and (*dashed line*) COT+TX ($y = –0.166x – 0.02$, $r^2 = 0.982$). The COT+NBA data could not be fitted to a linear expression.

Each of these PAs are amphiphiles, displaying varying degrees of hydrophobicity, which means that they may be expected to partition into the lipid bilayer and thus alter lipid bilayer properties (13,17), which would alter membrane protein function (16). PAs also may alter membrane protein function by binding directly to the protein—either in the substrate sites of the membrane protein or by interacting with sites that allosterically modulate function (e.g., Andersen (77)). It is in this context important that the gA channel structure, being an almost ideal cylinder (78–81), effectively precludes specific binding. The results obtained are parsimoniously explained by a model in which the PAs (except for DABCO) alter the energetic cost of bilayer deformation associated with gA channel formation.

TX, NBA, nPG, and pNBA increased the average number of gA channels/LUVs (Fig. 4), reflecting a shift in the gA monomer-dimer equilibrium toward the Tl^+-permeable dimer. That is, TX, NBA, nPG, and pNBA reduced the energetic cost of the bilayer deformation associated with gA channel formation. Such an effect would be similar to what has been observed with other amphiphiles (17,20–24,41,82–84), including short chain alcohols (14,85) and salicylate (15), where changes in bilayer properties reflect, at least in part, a decrease in bilayer bending stiffness.

The increased effect of pNBA at pH 4, as compared to pH 7, is similar to that observed for antifusion peptides (86), indicating that the neutral form of pNBA is a more potent bilayer modifier than the deprotonated/charged form. These results, however, are in contrast to observations made using straight-chain fatty acids, whether mono- or

polyunsaturated (87), suggesting that there may be a complex relationship between changes in charge and changes in bilayer-perturbing potency. Consistent with this notion, the alterations in gA activity observed for TX and NBA are similar, despite the fact that their structures and lipophilicity at neutral pH differ considerably (see Table S1 and Fig. S1). For the nonpolar COT molecule, the decreased gA channel activity (Fig. 4) reflects a shift the gA monomer-dimer equilibrium toward the nonconducting monomers that most likely is caused by its partitioning into the bilayer core to increase in bilayer thickness (88) and acyl-chain order (82). DABCO had no significant effect in channel activity, most likely owing to poor partitioning into the lipid membrane.

Assuming that the PAs do not interact directly with (bind to) the gA monomers or dimers, the changes in the free energy of channel formation can be attributed to the bilayer contribution to the energetic cost of dimer formation $\Delta G^{M\rightarrow D}_{bilayer}$ (16). Consistent with what has been observed for other amphiphiles (13–15,50), $\Delta\Delta G^{M\rightarrow D}_{bilayer}$ is reduced by the PAs TX, NBA, nPG, and pNBA, unaffected by DABCO and (somewhat surprisingly) increased by COT over the tested concentrations (Fig. 5). For the various compounds tested, $\Delta\Delta G^{M\rightarrow D}_{bilayer}$ varies linearly with [PA], and may exceed 2 k_BT. When we tested equimolar combinations of PAs (Fig. 6 and Fig. S7), $\Delta\Delta G^{M\rightarrow D}_{bilayer}$ similarly varied linearly with PA concentration (Fig. 6)—except for the COT+NBA mix where $\Delta\Delta G^{M\rightarrow D}_{bilayer}\approx 0$ with no systematic variation—and was consistently less than the sum of energies predicted from the experiments with the individual PAs (see Fig. S7). It thus appears to be advantageous to use combinations of PAs, as this will reduce the likelihood of membrane effects.

From the theory of elastic bilayer deformations (18), it can be concluded that $\Delta\Delta G^{M\rightarrow D}_{bilayer}$ will vary as an approximately linear function of channel (protein) radius (for a given channel-bilayer hydrophobic mismatch). The gA channel radius, ~10 Å, is less than the radius of most integral membrane proteins, but the channel-bilayer hydrophobic mismatch in the gA-LUV system is likely to be larger than for integral membrane proteins in biological membranes. Our results do not allow for direct comparison with integral membrane proteins—but a k_BT change in $\Delta G^{I\rightarrow II}_{bilayer}$ changes the I↔II equilibrium *e*-fold. The actual change in $\Delta G^{I\rightarrow II}_{bilayer}$ produced by a given PA will vary depending on the membrane protein conformational change and the properties of the host bilayer, but PAs cannot be assumed to be inert—and they should be assumed to alter membrane protein function at the concentrations where they alter the energetics of the gA monomer↔dimer equilibrium; see Lundbaek et al. (22) and Rusinova et al. (41).

These results demonstrate the importance of explicitly monitoring the bilayer-modifying potency of molecules used to explore the function of membrane proteins and cells. They further illustrate the complexities of associating a small molecule with its bilayer-modifying effects and, by extension, with its influence on membrane protein function. In cell and model membrane environments, amphiphiles may elicit a variety of unwanted effects due to their partitioning into the lipid bilayers. In this context, it is important that it is the energy on the entire bilayer/aqueous environment/membrane protein system that is minimized (46) and that the amphiphiles may redistribute in the membrane—being enriched (24) or depleted in the vicinity of the protein, as compared to the unperturbed bilayer. Additionally, interfacial effects such as pKa alterations (60) can alter the protonation states of the adsorbed species and by extension their effects on bilayer properties and protein function. Thus, an amphiphile's bilayer-modifying potency may not be predicted simply by its hydrophobicity, but may instead reflect complex interactions between the compound and the host bilayer (and the embedded proteins).

Synthetic cell membrane models and live cell imaging constitute a crucial frontier of fluorescence microscopy and spectroscopy. Understanding the effects of PAs and other additives on membrane properties, protein function, and organization will become increasingly important for the controlled study of membrane protein function and cell function in general. The unwanted effects of such compounds can be minimized by informed selection of the molecules employed and their working concentrations. Such effects also may be circumnavigated through the development of strategies in which PAs are directly or proximally conjugated to the fluorogenic center. Such pursuits, shown to be an effective means of enhancing the photostabilities of cyanine fluorophores (76,89), may provide a powerful approach for minimizing the risk of unwanted membrane effects.

SUPPORTING MATERIAL

Materials, methods, two tables, and seven figures are available at http://www.biophysj.org/biophysj/supplemental/S0006-3495(13)00472-4.

We thank R. Lea Sanford and Radda Rusinova for helpful discussions.

Reseach reported in this article was supported by the National Institute of General Medical Sciences of the National Institutes of Health under award numbers ROIGM21347 (to O.S.A.),ROIGM079238 and ROIGM098859 (both to S.C.B.). The content is solely the responsibility of the authors and does not necessarily represent the official views of the National Institutes of Health.

REFERENCES

1. Longin, A., C. Souchier, …, P. A. Bryon. 1993. Comparison of anti-fading agents used in fluorescence microscopy: image analysis and laser confocal microscopy study. *J. Histochem. Cytochem.* 41:1833–1840.

2. Widengren, J., A. Chmyrov, …, C. A. Seidel. 2007. Strategies to improve photostabilities in ultrasensitive fluorescence spectroscopy. *J. Phys. Chem. A.* 111:429–440.

3. Florijn, R. J., J. Slats, …, A. K. Raap. 1995. Analysis of antifading reagents for fluorescence microscopy. *Cytometry.* 19:177–182.
4. Dave, R., D. S. Terry, …, S. C. Blanchard. 2009. Mitigating unwanted photophysical processes for improved single-molecule fluorescence imaging. *Biophys. J.* 96:2371–2381.
5. Aitken, C. E., R. A. Marshall, and J. D. Puglisi. 2008. An oxygen scavenging system for improvement of dye stability in single-molecule fluorescence experiments. *Biophys. J.* 94:1826–1835.
6. Hübner, C. G., A. Renn, …, U. P. Wild. 2001. Direct observation of the triplet lifetime quenching of single dye molecules by molecular oxygen. *J. Chem. Phys.* 115:9619–9622.
7. Renn, A., J. Seelig, and V. Sandoghdar. 2006. Oxygen-dependent photochemistry of fluorescent dyes studied at the single molecule level. *Mol. Phys.* 104:409–414.
8. Rasnik, I., S. A. McKinney, and T. Ha. 2006. Nonblinking and long-lasting single-molecule fluorescence imaging. *Nat. Methods.* 3:891–893.
9. Dittrich, P. S., and P. Schwille. 2001. Photobleaching and stabilization of fluorophores used for single-molecule analysis with one- and two-photon excitation. *Appl. Phys. B.* 73:829–837.
10. Grunwell, J. R., J. L. Glass, …, P. G. Schultz. 2001. Monitoring the conformational fluctuations of DNA hairpins using single-pair fluorescence resonance energy transfer. *J. Am. Chem. Soc.* 123:4295–4303.
11. Pappalardo, R., H. Samelson, and A. Lempicki. 1970. Long-pulse laser emission from Rhodamine 6G. *IEEE J. Quantum Electron.* 6:716–725.
12. Cordes, T., I. H. Stein, …, P. Tinnefeld. 2009. Controlling the emission of organic dyes for high sensitivity and super-resolution microscopy. *Proc. SPIE*. http://dx.doi.org/10.1117/12.831495.
13. Evans, E., W. Rawicz, and A. F. Hofmann. 1995. Lipid bilayer expansion and mechanical disruption in solutions of water-soluble bile acid. *In* Bile Acids in Gastroenterology: Basic and Clinical Advances. A. F. Hofmann, B. Paumgartner, and A. Stiehl, editors.. Kluwer Academic Publishers, San Diego, CA. 59–68.
14. Ly, H. V., and M. L. Longo. 2004. The influence of short-chain alcohols on interfacial tension, mechanical properties, area/molecule, and permeability of fluid lipid bilayers. *Biophys. J.* 87:1013–1033.
15. Zhou, Y., and R. M. Raphael. 2005. Effect of salicylate on the elasticity, bending stiffness, and strength of SOPC membranes. *Biophys. J.* 89:1789–1801.
16. Lundbaek, J. A., S. A. Collingwood, …, O. S. Andersen. 2010. Lipid bilayer regulation of membrane protein function: gramicidin channels as molecular force probes. *J. R. Soc. Interface.* 7:373–395.
17. Lundbaek, J. A., and O. S. Andersen. 1994. Lysophospholipids modulate channel function by altering the mechanical properties of lipid bilayers. *J. Gen. Physiol.* 104:645–673.
18. Nielsen, C., and O. S. Andersen. 2000. Inclusion-induced bilayer deformations: effects of monolayer equilibrium curvature. *Biophys. J.* 79:2583–2604.
19. Andersen, O. S., and R. E. Koeppe, 2nd. 2007. Bilayer thickness and membrane protein function: an energetic perspective. *Annu. Rev. Biophys. Biomol. Struct.* 36:107–130.
20. Hwang, T. C., R. E. Koeppe, 2nd, and O. S. Andersen. 2003. Genistein can modulate channel function by a phosphorylation-independent mechanism: importance of hydrophobic mismatch and bilayer mechanics. *Biochemistry.* 42:13646–13658.
21. Lundbaek, J. A., P. Birn, …, O. S. Andersen. 2004. Regulation of sodium channel function by bilayer elasticity: the importance of hydrophobic coupling. Effects of micelle-forming amphiphiles and cholesterol. *J. Gen. Physiol.* 123:599–621.
22. Lundbaek, J. A., P. Birn, …, O. S. Andersen. 2005. Capsaicin regulates voltage-dependent sodium channels by altering lipid bilayer elasticity. *Mol. Pharmacol.* 68:680–689.
23. Artigas, P., S. J. Al'aref, …, O. S. Andersen. 2006. 2,3-butanedione monoxime affects cystic fibrosis transmembrane conductance regulator channel function through phosphorylation-dependent and phosphorylation-independent mechanisms: the role of bilayer material properties. *Mol. Pharmacol.* 70:2015–2026.
24. Bruno, M. J., R. E. Koeppe, 2nd, and O. S. Andersen. 2007. Docosahexaenoic acid alters bilayer elastic properties. *Proc. Natl. Acad. Sci. USA.* 104:9638–9643.
25. Gustafsson, M. G., L. Shao, …, J. W. Sedat. 2008. Three-dimensional resolution doubling in wide-field fluorescence microscopy by structured illumination. *Biophys. J.* 94:4957–4970.
26. Mittal, A., E. Leikina, …, J. Bentz. 2003. Kinetically differentiating influenza hemagglutinin fusion and hemifusion machines. *Biophys. J.* 85:1713–1724.
27. Bischofs, I. B., F. Klein, …, U. S. Schwarz. 2008. Filamentous network mechanics and active contractility determine cell and tissue shape. *Biophys. J.* 95:3488–3496.
28. Lee, J., Y. Miyanaga, …, S. Hohng. 2012. Video-rate confocal microscopy for single-molecule imaging in live cells and superresolution fluorescence imaging. *Biophys. J.* 103:1691–1697.
29. Scriven, D. R., P. Asghari, …, E. D. Moore. 2010. Analysis of Cav1.2 and ryanodine receptor clusters in rat ventricular myocytes. *Biophys. J.* 99:3923–3929.
30. Bethge, P., R. Chéreau, …, U. V. Nägerl. 2013. Two-photon excitation STED microscopy in two colors in acute brain slices. *Biophys. J.* 104:778–785.
31. Sakon, J. J., and K. R. Weninger. 2010. Detecting the conformation of individual proteins in live cells. *Nat. Methods.* 7:203–205.
32. Lovrić, J., H. S. Bazzi, …, D. Maysinger. 2005. Differences in subcellular distribution and toxicity of green and red emitting CdTe quantum dots. *J. Mol. Med.* 83:377–385.
33. Li, Y., G. J. Augustine, and K. Weninger. 2007. Kinetics of complexin binding to the SNARE complex: correcting single molecule FRET measurements for hidden events. *Biophys. J.* 93:2178–2187.
34. Pontani, L. L., J. van der Gucht, …, C. Sykes. 2009. Reconstitution of an actin cortex inside a liposome. *Biophys. J.* 96:192–198.
35. Zhao, J., J. Wu, …, G. Feigenson. 2007. Phase studies of model biomembranes: macroscopic coexistence of $L\alpha + L\beta$, with light-induced coexistence of $L\alpha + L_o$ phases. *Biochim. Biophys. Acta.* 1768:2777–2786.
36. Ira, S., S. Zou, …, L. J. Johnston. 2009. Enzymatic generation of ceramide induces membrane restructuring: correlated AFM and fluorescence imaging of supported bilayers. *J. Struct. Biol.* 168:78–89.
37. Choi, U. B., P. Strop, …, K. R. Weninger. 2010. Single-molecule FRET-derived model of the synaptotagmin 1-SNARE fusion complex. *Nat. Struct. Mol. Biol.* 17:318–324.
38. Bowen, M. E., K. Weninger, …, A. T. Brunger. 2005. Single-molecule studies of synaptotagmin and complexin binding to the SNARE complex. *Biophys. J.* 89:690–702.
39. Lundbaek, J. A., P. Birn, …, O. S. Andersen. 1996. Membrane stiffness and channel function. *Biochemistry.* 35:3825–3830.
40. Ingólfsson, H. I., and O. S. Andersen. 2010. Screening for small molecules' bilayer-modifying potential using a gramicidin-based fluorescence assay. *Assay Drug Dev. Technol.* 8:427–436.
41. Rusinova, R., K. F. Herold, …, O. S. Andersen. 2011. Thiazolidinedione insulin sensitizers alter lipid bilayer properties and voltage-dependent sodium channel function: implications for drug discovery. *J. Gen. Physiol.* 138:249–270.
42. Elliott, J. R., D. Needham, …, D. A. Haydon. 1983. The effects of bilayer thickness and tension on gramicidin single-channel lifetime. *Biochim. Biophys. Acta.* 735:95–103.
43. Huang, H. W. 1986. Deformation free energy of bilayer membrane and its effect on gramicidin channel lifetime. *Biophys. J.* 50:1061–1070.
44. Harroun, T. A., W. T. Heller, …, H. W. Huang. 1999. Experimental evidence for hydrophobic matching and membrane-mediated interactions in lipid bilayers containing gramicidin. *Biophys. J.* 76:937–945.
45. Jones, T. L., R. Fu, …, D. D. Busath. 2010. Gramicidin channels are internally gated. *Biophys. J.* 98:1486–1493.

46. Andersen, O. S., D. B. Sawyer, and R. E. I. Koeppe. 1992. Modulation of channel function by the host bilayer. *In* Biomembrane Structure and Function. B. Gaber and K. R. K. Easwaran, editors.. Adenine Press, Schenectady, NY. 227–244.

47. Kemp, G., and C. Wenner. 1976. Solution, interfacial, and membrane properties of gramicidin A. *Arch. Biochem. Biophys.* 176:547–555.

48. Bruggemann, E. P., and C. Kayalar. 1986. Determination of the molecularity of the colicin E1 channel by stopped-flow ion flux kinetics. *Proc. Natl. Acad. Sci. USA.* 83:4273–4276.

49. Lum, K., H. I. Ingolfsson, …, O. S. Andersen. 2011. Exchange of gramicidin between lipid bilayers: implications for the mechanism of channel formation and gating. *Biophys. J.* 100:501a.

50. Zhelev, D. V. 1998. Material property characteristics for lipid bilayers containing lysolipid. *Biophys. J.* 75:321–330.

51. Hope, M. J., M. B. Bally, …, P. R. Cullis. 1985. Production of large unilamellar vesicles by a rapid extrusion procedure: characterization of size distribution, trapped volume and ability to maintain a membrane potential. *Biochim. Biophys. Acta.* 812:55–65.

52. Peiró-Salvador, T., O. Ces, …, A. M. Seddon. 2009. Buffers may adversely affect model lipid membranes: a cautionary tale. *Biochemistry.* 48:11149–11151.

53. Schwarz, G., and C. H. Robert. 1992. Kinetics of pore-mediated release of marker molecules from liposomes or cells. *Biophys. Chem.* 42:291–296.

54. Peyron, M., G. K. Pierens, …, R. C. Stewart. 1996. The modified stretched-exponential model for characterization of NMR relaxation in porous media. *J. Magn. Reson. A.* 118:214–220.

55. Berberan-Santos, M. N., E. N. Bodunov, and B. Valeur. 2005. Mathematical functions for the analysis of luminescence decays with underlying distributions 1. Kohlrausch decay function (stretched exponential). *Chem. Phys.* 315:171–182.

56. Martinus, N., and C. A. Vincent. 1976. Viscosity of aqueous solutions of $TlNO_3$, $Tl2SO_4$ and TlOH at 25°C. *J. Am. Chem. Soc., Faraday Trans. I.* 72:2505–2511.

57. Kolthoff, I. M., and J. M. K. Chantooni. 1980. Transfer activity coefficients in various solvents of several univalent cations complexed with dibenzo-18-crown-6. *Anal. Chem.* 52:1039–1044.

58. Cordes, T., J. Vogelsang, and P. Tinnefeld. 2009. On the mechanism of Trolox as antiblinking and antibleaching reagent. *J. Am. Chem. Soc.* 131:5018–5019.

59. Braude, E. A., and F. C. Nachod. 1955. Determination of Organic Structures by Physical Methods. Academic Press, New York.

60. Drummond, C. J., F. Grieser, and T. W. Healy. 1989. Acid-base equilibria in aqueous micellar solutions. Part 1. 'Simple' weak acids and bases. *J. Chem. Soc., Faraday Trans. I.* 85:521–535.

61. Peitzsch, R. M., and S. McLaughlin. 1993. Binding of acylated peptides and fatty acids to phospholipid vesicles: pertinence to myristoylated proteins. *Biochemistry.* 32:10436–10443.

62. Froud, R. J., J. M. East, …, A. G. Lee. 1986. Binding of long-chain alkyl derivatives to lipid bilayers and to (Ca^{2+}-Mg^{2+})-ATPase. *Biochemistry.* 25:7535–7544.

63. Von Trebra, R., and T. H. Koch. 1982. DABCO stabilization of coumarin dye lasers. *Chem. Phys. Lett.* 93:315–317.

64. Johnson, G. D., R. S. Davidson, …, E. J. Holborow. 1982. Fading of immunofluorescence during microscopy: a study of the phenomenon and its remedy. *J. Immunol. Methods.* 55:231–242.

65. Gaigalas, A. K., L. Wang, …, E. Humphries. 2004. Photodegradation of fluorescein in solutions containing n-propyl gallate. *J. Phys. Chem. A.* 108:4378–4384.

66. Berrios, M., K. A. Conlon, and D. E. Colflesh. 1999. Antifading agents for confocal fluorescence microscopy. *Methods Enzymol.* 307:55–79.

67. Giloh, H., and J. W. Sedat. 1982. Fluorescence microscopy: reduced photobleaching of Rhodamine and fluorescein protein conjugates by *n*-propyl gallate. *Science.* 217:1252–1255.

68. Inoue, K., T. Tsurumi, …, K. Ikeda. 2012. Cytological evaluation of the effect of azoxystrobin and alternative oxidase inhibitors in *Botrytis cinerea*. *FEMS Microbiol. Lett.* 326:83–90.

69. Jung, H. J., and C. J. Lim. 2011. The antiangiogenic and antinociceptive activities of *n*-propyl gallate. *Phytother. Res.* 25:1570–1573.

70. You, B. R., and W. H. Park. 2011. The enhancement of propyl gallate-induced apoptosis in HeLa cells by a proteasome inhibitor MG132. *Oncol. Rep.* 25:871–877.

71. Chang, Y. J., Y. P. Huang, …, C. H. Chen. 2012. GRP78 knockdown enhances apoptosis via the down-regulation of oxidative stress and Akt pathway after epirubicin treatment in colon cancer DLD-1 cells. *PLoS ONE.* 7:e35123.

72. D'Agostino, D. P., J. E. Olson, and J. B. Dean. 2009. Acute hyperoxia increases lipid peroxidation and induces plasma membrane blebbing in human U87 glioblastoma cells. *Neuroscience.* 159:1011–1022.

73. Dang, T. N., G. M. Bishop, …, S. R. Robinson. 2011. The metabolism and toxicity of hemin in astrocytes. *Glia.* 59:1540–1550.

74. Horn, A. P., A. Bernardi, …, C. Salbego. 2011. Mesenchymal stem cell-conditioned medium triggers neuroinflammation and reactive species generation in organotypic cultures of rat hippocampus. *Stem Cells Dev.* 20:1171–1181.

75. Choi, E. M. 2012. Regulation of intracellular Ca^{2+} by reactive oxygen species in osteoblasts treated with antimycin A. *J. Appl. Toxicol.* 32:118–125.

76. Altman, R. B., D. S. Terry, …, S. C. Blanchard. 2012. Cyanine fluorophore derivatives with enhanced photostability. *Nat. Methods.* 9:68–71.

77. Andersen, O. S. 2008. Perspectives on how to drug an ion channel. *J. Gen. Physiol.* 131:395.

78. Arseniev, A. S., I. L. Barsukov, …, Yu. A. Ovchinnikov. 1985. 1H-NMR study of gramicidin A transmembrane ion channel. Head-to-head right-handed, single-stranded helices. *FEBS Lett.* 186:168–174.

79. Ketchem, R., B. Roux, and T. Cross. 1997. High-resolution polypeptide structure in a lamellar phase lipid environment from solid state NMR derived orientational constraints. *Structure.* 5:1655–1669.

80. Townsley, L. E., W. A. Tucker, …, J. F. Hinton. 2001. Structures of gramicidins A, B, and C incorporated into sodium dodecyl sulfate micelles. *Biochemistry.* 40:11676–11686.

81. Allen, T. W., O. S. Andersen, and B. Roux. 2003. Structure of gramicidin a in a lipid bilayer environment determined using molecular dynamics simulations and solid-state NMR data. *J. Am. Chem. Soc.* 125:9868–9877.

82. Ingólfsson, H. I., and O. S. Andersen. 2011. Alcohol's effects on lipid bilayer properties. *Biophys. J.* 101:847–855.

83. Sawyer, D. B., and O. S. Andersen. 1989. Platelet-activating factor is a general membrane perturbant. *Biochim. Biophys. Acta.* 987:129–132.

84. Sawyer, D. B., R. E. Koeppe, 2nd, and O. S. Andersen. 1989. Induction of conductance heterogeneity in gramicidin channels. *Biochemistry.* 28:6571–6583.

85. Ly, H. V., D. E. Block, and M. L. Longo. 2002. Interfacial tension effect of ethanol on lipid bilayer rigidity, stability, and area/molecule: a micropipet aspiration approach. *Langmuir.* 18:8988–8995.

86. Ashrafuzzaman, M., M. A. Lampson, …, O. S. Andersen. 2006. Manipulating lipid bilayer material properties using biologically active amphipathic molecules. *J. Phys. Condens. Matter.* 18:S1235–S1255.

87. Bruno, M. J., R. Rusinova, …, O. S. Andersen. 2013. Interactions of drugs and amphiphiles with membranes. Modulation of lipid bilayer elastic properties by changes in acyl chain unsaturation and protonation. *Faraday Discuss.* 161:461–480.

88. Kolb, H. A., and E. Bamberg. 1977. Influence of membrane thickness and ion concentration on the properties of the gramicidin a channel. Autocorrelation, spectral power density, relaxation and single-channel studies. *Biochim. Biophys. Acta.* 464:127–141.

89. Altman, R. B., Q. Zheng, …, S. C. Blanchard. 2012. Enhanced photostability of cyanine fluorophores across the visible spectrum. *Nat. Methods.* 9:428–429.